Research Square

Preprints are preliminary reports that have not undergone peer review.
They should not be considered conclusive, used to inform clinical practice,
or referenced by the media as validated information.

De novo DSG2 p.His361Arg in an oligogenic background of severe biventricular arrhythmogenic cardiomyopathy: clinical, familial, and molecular dynamics evidence

Ming Zhang
The Second Hospital of Jilin University, Jilin University
Ziyuan Guo
The Second Hospital of Jilin University, Jilin University
Lirui Kang
The Second Hospital of Jilin University, Jilin University
Tianyi Li
The Second Hospital of Jilin University, Jilin University
Yinuo Guan
The Second Hospital of Jilin University, Jilin University
Kang LV
The Second Hospital of Jilin University, Jilin University
Ziyan Jiao
The Second Hospital of Jilin University, Jilin University
Jichang Zhang
jichang@jlu.edu.cn

The Second Hospital of Jilin University, Jilin University

Research Article

Keywords: arrhythmogenic cardiomyopathy, arrhythmogenic right ventricular cardiomyopathy, DSG2, FLNC, TTN, oligogenic inheritance, molecular dynamics simulation

Posted Date: November 25th, 2026

DOI: https://doi.org/10.21203/rs.3.rs-11511427/v1

License: This work is licensed under a Creative Commons Attribution 4.0 International License.
Read Full License

Additional Declarations: No competing interests reported.

De novo DSG2 p.His361Arg in an oligogenic background of severe biventricular arrhythmogenic cardiomyopathy: clinical, familial, and molecular dynamics evidence

Ming Zhang[1,#], Ziyuan Guo[1,#], Lirui Kang[1], Tianyi Li[1], Yinuo Guan[1], Kang LV[1], Ziyan Jiao[1], Jichang Zhang[1,*]

1 Cardiology Department, The Second Hospital of Jilin University, Jilin University, Changchun 130041, China

*Corresponding author: Jichang Zhang

Cardiology Department, The Second Hospital of Jilin University, Jilin University, No. 4026 Yatai Street, Nanguan District, Changchun City, Jilin Province, 130041, China,

Fax: +86-0431-81136599; Tel: +86-0431-81136598; E-mail: jichang@jlu.edu.cn

[#] Ming Zhang and Ziyuan Guo contributed equally to this work

Abstract

Background: Arrhythmogenic right ventricular cardiomyopathy is now recognized within the broader spectrum of arrhythmogenic cardiomyopathy. Desmosomal variants are central to disease pathogenesis, but penetrance and severity can vary markedly even within families. This report was restructured around a hierarchical genetic model in which DSG2 is treated as the primary disease-associated gene and inherited FLNC and TTN variants are evaluated as candidate phenotypic modifiers.

Case presentation: A 22-year-old man had exercise-associated syncope at age 17 and later developed exertional dyspnea and palpitations. Electrocardiography showed incomplete right bundle branch block, low voltage in V1 to V3, and T-wave inversion in V1 to V6. Twenty-four-

hour monitoring recorded 4,037 premature ventricular contractions and ventricular tachycardia. Echocardiography demonstrated marked right ventricular outflow tract enlargement and a fractional area change of 3.87%. Cardiac magnetic resonance showed severe right ventricular enlargement and dysfunction, with an end-diastolic volume of 311 mL and an ejection fraction of 3.69%, together with left ventricular dysfunction with an ejection fraction of 39.86%.

Genetic and molecular analysis: Family testing identified DSG2 NM_001943.5:c.1082A>G, p.His361Arg only in the proband, whereas FLNC NM_001458.5:c.1042C>T, p.His348Tyr and TTN NM_001267550.2:c.39990G>T, p.Lys13330Asn were shared with the clinically unaffected father. His361 is located in the extracellular cadherin region of DSG2 and is conserved in the examined mammalian orthologues. A nearby EC3 variant, p.Ala358Thr, has been reported in a compound DSG2 genotype associated with early biventricular disease. Molecular dynamics simulations showed that DSG2 p.His361Arg preserved the global fold but reorganized the local hydrogen-bond network and broadened conformational sampling. FLNC p.His348Tyr showed local interaction strengthening with reduced local flexibility. TTN p.Lys13330Asn altered local polar interactions and broadened conformational sampling within the modeled fragment.

Conclusion: The combined clinical, segregation, structural-context, and molecular-dynamics evidence supports DSG2 p.His361Arg as the principal disease-associated candidate in this family. The inherited FLNC and TTN variants are more appropriately interpreted as candidate modifiers than as independently causative variants. This oligogenic model is biologically plausible but remains a hypothesis that requires experimental functional validation.

Keywords: arrhythmogenic cardiomyopathy; arrhythmogenic right ventricular cardiomyopathy; DSG2; FLNC; TTN; oligogenic inheritance; molecular dynamics simulation

Introduction

Arrhythmogenic cardiomyopathy is an inherited myocardial disease characterized by ventricular arrhythmias, progressive ventricular dysfunction, and an increased risk of sudden cardiac death. The traditional right ventricular phenotype remains clinically important, but contemporary diagnostic frameworks recognize right-dominant, biventricular, and left-dominant forms [1]. The 2010 Task Force Criteria remain widely used for classical arrhythmogenic right ventricular cardiomyopathy and integrate structural, electrocardiographic, arrhythmic, histological, and familial findings [2]. Contemporary consensus statements emphasize multimodality imaging, genetic evaluation, exercise counseling, and individualized sudden-death risk assessment [3]. The 2023 European Society of Cardiology guideline further places genotype and phenotype within a longitudinal cardiomyopathy framework rather than treating genetic results as isolated diagnostic labels [4].

The genetic basis of arrhythmogenic cardiomyopathy is heterogeneous. Evidence-based ClinGen reassessment has confirmed a core group of genes with strong or definitive relationships to classical arrhythmogenic right ventricular cardiomyopathy, including the desmosomal gene DSG2 [5]. DSG2 encodes desmoglein 2, the only desmoglein isoform expressed in cardiomyocytes. Pathogenic DSG2 variants were established early in the molecular characterization of arrhythmogenic right ventricular cardiomyopathy [6]. Structural studies show that the DSG2 ectodomain is formed by tandem extracellular cadherin domains that support calcium-dependent adhesion and transmit mechanical stress across the desmosome [7]. These observations make a newly identified DSG2 missense variant biologically credible, but the credibility of the gene does not automatically establish the pathogenicity of an individual amino-acid substitution.

This distinction is particularly important for missense variants. A recent integrative analysis of 115 studies and 145 curated DSG2 variants showed that clinically important missense variants are enriched in extracellular domains, while many other missense substitutions remain variants of uncertain significance [8]. Functional studies of DSG2-associated variants have also shown that impaired cadherin binding kinetics can occur without destruction of the global protein architecture [9]. More recent biophysical work similarly supports the concept that altered desmosomal binding dynamics may be a meaningful mechanism in arrhythmogenic cardiomyopathy [10]. Therefore, evaluation of a novel DSG2 missense substitution should consider segregation, conservation, structural location, nearby disease-associated variants, and dynamic effects rather than relying only on generic prediction scores.

The genetic architecture may also be more complex than a single-variant model. Compound and digenic heterozygosity has been documented in arrhythmogenic right ventricular cardiomyopathy [11]. Family studies have shown that relatives carrying more than one relevant variant can have greater disease penetrance than relatives with a single variant [12]. Multiple desmosomal variants have been associated with more extensive repolarization abnormalities and left ventricular involvement [13]. Complex genotypes have also been linked to a higher lifetime arrhythmic risk [14]. However, such observations cannot be transferred uncritically to variants in genes with different disease-validity evidence. FLNC truncating variants are strongly associated with high-risk dilated and arrhythmogenic cardiomyopathy phenotypes [15], and FLNC truncations have also been described in right ventricular arrhythmogenic cardiomyopathy [16]. By contrast, TTN is firmly established in dilated cardiomyopathy [17], while its proposed relationship with classical arrhythmogenic right ventricular cardiomyopathy has been classified as disputed by ClinGen [18].

The present report was therefore designed around a hierarchical interpretation. DSG2 p.His361Arg was evaluated as the principal disease-associated candidate. The paternally inherited FLNC p.His348Tyr and TTN p.Lys13330Asn variants were evaluated as possible modifiers. The analysis was extended beyond routine in silico prediction by examining DSG2 sequence conservation and regional literature context and by integrating molecular dynamics simulations of all three substitutions. The central question was not whether each variant could be labeled pathogenic from computational data alone. The objective was to determine whether the clinical, familial, structural, and dynamic evidence formed a coherent mechanistic explanation for the unusually early and severe biventricular phenotype.

Methods

Study design and clinical assessment

This single-case investigation integrated clinical phenotyping, family-based genetic assessment, sequence conservation and regional structural analysis, and molecular dynamics simulations. Clinical information was obtained from the proband's documented history and admission assessment. Electrocardiography and 24-hour Holter monitoring were reviewed to characterize electrical abnormalities and ventricular arrhythmias. Transthoracic echocardiography and cardiac magnetic resonance imaging were evaluated for ventricular dimensions, regional wall motion, and systolic function. The clinical phenotype was assessed using the 2010 Task Force Criteria for arrhythmogenic right ventricular cardiomyopathy [2], while left ventricular involvement was considered in the broader arrhythmogenic cardiomyopathy context.

Genetic testing and family segregation analysis

Whole-exome sequencing was conducted as part of the clinical genetic evaluation. The three variants subsequently examined were DSG2 NM_001943.5:c.1082A>G, p.His361Arg; FLNC NM_001458.5:c.1042C>T, p.His348Tyr; and TTN NM_001267550.2:c.39990G>T, p.Lys13330Asn. Family testing included the proband, father, mother, and sister. Sanger sequencing chromatograms were used to document the selected substitutions, and the genotypes were compared with the reported clinical status of family members. The interpretation distinguished a principal disease-associated candidate from potential modifier variants, rather than assuming independent causality for all three substitutions.

Sequence conservation and structural-context analysis

The amino-acid region surrounding DSG2 His361 was examined using the human UniProt sequence Q14126 and the corresponding orthologous sequences from mouse O55111 and pig A0A287ATF2. The local sequence segments were compared to assess conservation of His361. The residue was mapped to the extracellular cadherin region of DSG2, and previously reported variants in the neighboring EC3 region were reviewed to provide positional and disease-context information. The literature-based and structural-context findings were considered supportive evidence and were not used alone to establish variant pathogenicity.

Molecular dynamics simulations and trajectory analysis

The molecular dynamics protocol was retained from the supplied simulation report and was checked for consistency with the protein assignments. Human DSG2 was obtained from UniProt Q14126. The three-dimensional starting structure was PDB 5ERD, chain A. The p.His361Arg substitution was introduced in PyMOL. FLNC was based on UniProt Q14315, and residues 33 to 368 were used for the p.His348Tyr model. For TTN, residues 13,299 to 13,384 were modeled

with SWISS-MODEL, and p.Lys13330Asn was introduced into the resulting fragment [22]. Structural inspection and energy minimization were performed with UCSF Chimera using the AMBER14SB force field [23]. Variant structures were generated with PyMOL [24].

Simulations were performed in GROMACS 2022.4 with the AMBER14SB force field [25]. TIP3P water and 0.15 mol/L sodium chloride were used. Energy minimization consisted of 10,000 steepest-descent steps followed by 5,000 conjugate-gradient steps. Each system then underwent 500 ps of NVT equilibration and 500 ps of NPT equilibration before a 100 ns production simulation. Temperature was maintained at 298.15 K with velocity rescaling [26]. Pressure was maintained at 1 bar with the Parrinello-Rahman method [27]. The integration time step was 2 fs. Long-range electrostatics were treated by particle-mesh Ewald, and 12 Å cutoffs were used for Coulombic and van der Waals interactions [28]. Hydrogen-containing covalent bonds were constrained with LINCS.

Trajectory analyses included backbone root mean square deviation, residue root mean square fluctuation, radius of gyration, solvent-accessible surface area, global and local hydrogen bonding, local contacts within 0.35 nm of the variant site, principal component analysis, Gibbs free-energy landscapes, representative low-energy structures, and secondary-structure evolution. The supplied analysis represents one 100 ns production trajectory per wild-type or mutant system. No independent replicate trajectories were present in the source materials. Consequently, the analyses were interpreted qualitatively and mechanistically rather than as replicate-level statistical evidence.

Case Presentation

Clinical course

The proband was a 22-year-old man. At age 17, he developed sudden syncope with brief loss of consciousness after strenuous exercise. Spontaneous recovery occurred within seconds. There was no reported urinary or fecal incontinence. Approximately two years before the current admission, exertional chest tightness, dyspnea, and palpitations developed. The symptoms improved with rest and had not previously prompted systematic treatment. He was admitted after abnormalities on electrocardiography and echocardiography raised suspicion of arrhythmogenic right ventricular cardiomyopathy.

On admission, height was 176 cm and weight was 86 kg. Blood pressure was 120/75 mmHg. Heart rate was 52 beats/min. The rhythm was irregular, and premature beats were audible. The right cardiac border was enlarged. Serum electrolytes, liver function, renal function, and thyroid function were reported as normal.

Electrophysiological phenotype

The admission electrocardiogram showed sinus bradycardia and incomplete right bundle branch block with a QRS duration of 112 ms. Low voltage was present in V1 to V3. T-wave inversion extended from V1 to V6. Twenty-four-hour Holter monitoring recorded 4,037 premature ventricular contractions and ventricular tachycardia. The source report described the ventricular tachycardia as arising from the apical region. The available tracing does not provide sufficient information to independently classify the ventricular tachycardia morphology according to the 2010 Task Force Criteria. The burden of more than 500 premature ventricular contractions per 24 hours nevertheless satisfies an arrhythmic minor criterion [20]. Epsilon waves were not clearly identified. This is not unexpected because their detection is technically sensitive and

interobserver reproducibility is limited [21]. The electrocardiographic findings, Holter tracing, and clinical timeline are presented in Fig. 1.

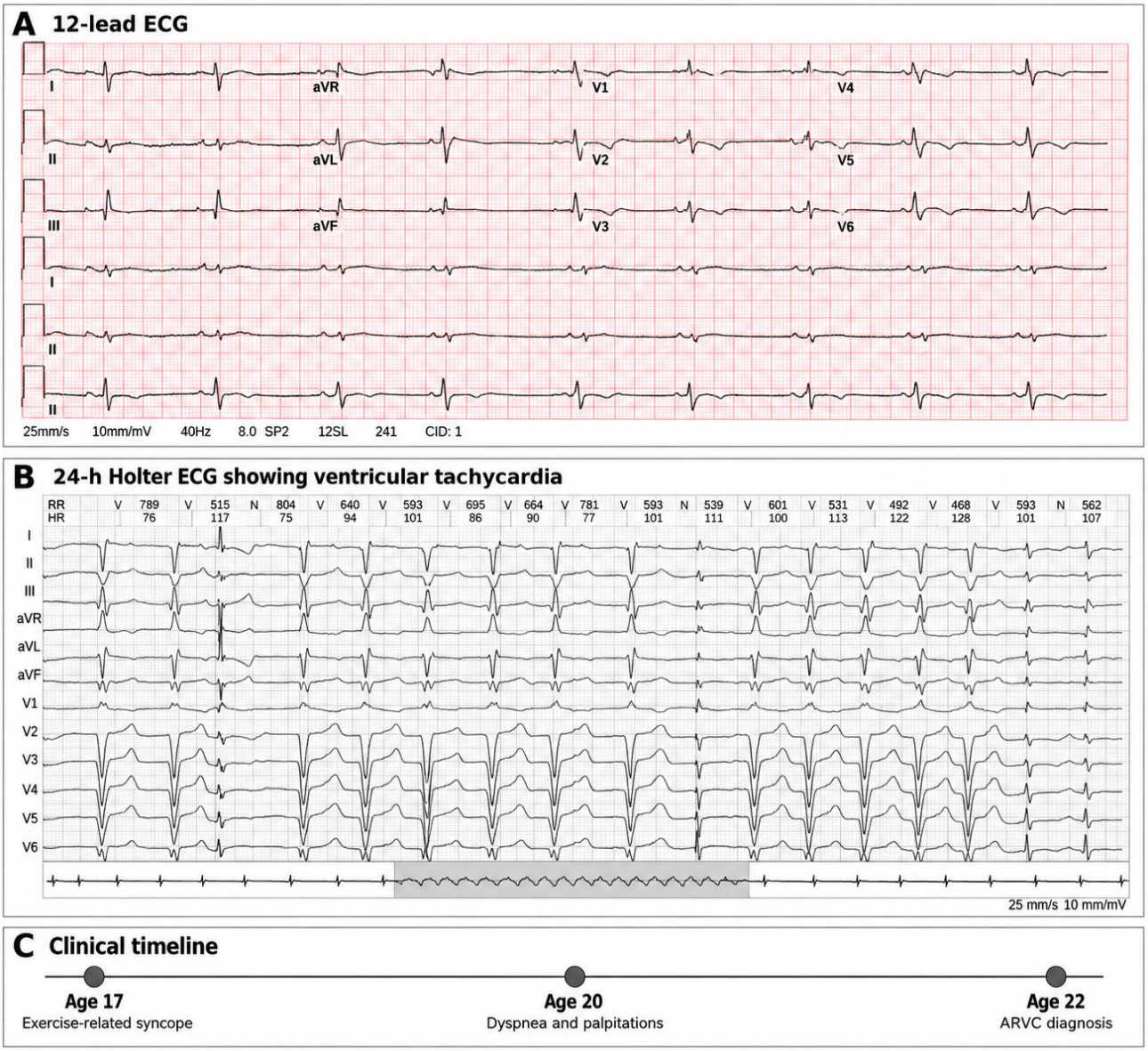

Figure 1. Electrical phenotype and clinical course. Panels A and B reproduce the original electrocardiographic and Holter data supplied with the case. Panel C summarizes the clinical timeline. The experimental tracings were not regenerated or altered.

Cardiac imaging and diagnostic interpretation

Echocardiography showed marked right ventricular outflow tract enlargement. The parasternal long-axis right ventricular outflow tract diameter was 57 mm, with an indexed value of 28.22 mm/m². The parasternal short-axis diameter was 48 mm, with an indexed value of 23.76 mm/m². Right ventricular fractional area change was 3.87%, and diffuse right ventricular wall-motion impairment was reported. Mild tricuspid regurgitation was present. The left ventricle was mildly enlarged and had reduced systolic function, with an ejection fraction of approximately 45%. A small pericardial effusion was also reported.

Cardiac magnetic resonance imaging showed severe right ventricular enlargement, an anteroposterior diameter of 67 mm, wall thinning, abnormal wall motion, and patchy fatty signal in the right ventricular wall. Right ventricular end-diastolic volume was 311 mL. Right ventricular end-systolic volume was 299 mL. Right ventricular ejection fraction was 3.69%. Indexed right ventricular end-diastolic volume was 153.96 mL/m². The left ventricle was also enlarged. Left ventricular end-diastolic volume was 168 mL, end-systolic volume was 101 mL, and left ventricular ejection fraction was 39.86%. Cardiac magnetic resonance is particularly valuable in arrhythmogenic cardiomyopathy because it provides reproducible assessment of right ventricular volumes, function, regional wall motion, and tissue characteristics [19].

The combination of repolarization abnormalities, frequent ventricular ectopy, ventricular tachycardia, marked right ventricular enlargement, severe right ventricular systolic dysfunction, and regional wall-motion abnormalities was considered diagnostic of classical arrhythmogenic right ventricular cardiomyopathy under the 2010 Task Force framework. The marked left ventricular dysfunction indicates a clinically important biventricular phenotype. Importantly, the diagnosis does not depend on treating the novel DSG2 missense variant as an already established

pathogenic variant. The echocardiographic and cardiac magnetic resonance findings are illustrated in Fig. 2. Their diagnostic relevance is summarized in Table 1.

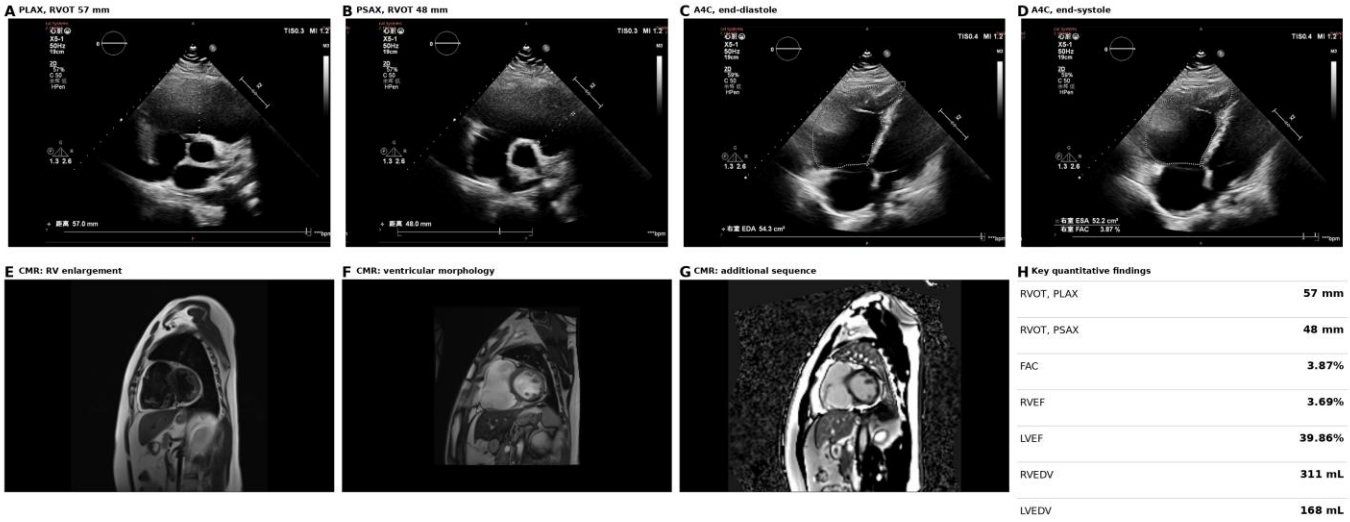

Figure 2. Biventricular structural and functional phenotype. Panels A to D reproduce the original echocardiographic images. Panels E to G reproduce the original cardiac magnetic resonance images. Panel H summarizes the quantitative measurements reported in the source manuscript. No clinical image was synthetically regenerated.

Table 1. Phenotype characterization and diagnostic relevance. The table separates the clinical diagnosis from the later mechanistic interpretation of the genetic findings.

Domain	Observed finding	Interpretive relevance
Repolarization	T-wave inversion in V1 to V6 at age 22 without complete right bundle branch block	Strongly supports the ARVC phenotype and exceeds the distribution required for a major repolarization criterion.
Arrhythmia	4,037 premature ventricular contractions in 24 hours; ventricular tachycardia documented	The ectopic burden exceeds the 2010 minor-criterion threshold. VT morphology was not fully classifiable from the supplied data.
Echocardiography	PLAX RVOT 57 mm; PLAX/BSA 28.22 mm/m²; PSAX RVOT 48 mm; PSAX/BSA 23.76 mm/m²; FAC 3.87%	Severe right ventricular enlargement and systolic dysfunction. Quantitative values are well beyond major-threshold ranges; formal scoring also requires the specified regional wall-motion abnormality.
Cardiac magnetic resonance	RVEDV 311 mL; RVEDVi 153.96 mL/m²; RVEF 3.69%; abnormal wall motion; LVEDV 168 mL; LVEF 39.86%	Advanced right ventricular disease with concomitant left ventricular involvement, consistent with a biventricular ACM phenotype.
Genetics	Novel DSG2 missense variant plus paternal FLNC and TTN variants	Supports etiologic investigation but should not be used as an independent major genetic criterion until variant classification is adequately established.

Genetic and Bioinformatic Results

Variant detection and family segregation

Whole-exome sequencing was performed as part of the clinical genetic evaluation. The proband carried three heterozygous missense variants. These were DSG2 NM_001943.5:c.1082A>G, p.His361Arg; FLNC NM_001458.5:c.1042C>T, p.His348Tyr; and TTN NM_001267550.2:c.39990G>T, p.Lys13330Asn. The gene and transcript assignments were rechecked during the present revision because FLNC and TTN had been interchanged in the earlier manuscript draft. Family validation showed that DSG2 p.His361Arg was not detected in the tested father, mother, or sister. FLNC p.His348Tyr and TTN p.Lys13330Asn were present in the father and proband but not in the mother or sister. The father was reported to have no overt cardiomyopathy.

This segregation pattern is the key observation underlying the revised model. The proband and father share the FLNC and TTN variants, but only the proband carries DSG2 p.His361Arg and manifests severe early disease. The pattern is therefore more consistent with DSG2 as the principal candidate and FLNC and TTN as potential modifiers than with an assumption that all three variants are independently pathogenic. The absence of the DSG2 variant from the tested parents is compatible with a de novo event within the tested family. Formal assignment of strong de novo evidence requires confirmation of biological parentage, which was not documented in the supplied materials. The pedigree, Sanger sequencing findings, and genotype–phenotype segregation are shown in Fig. 3.

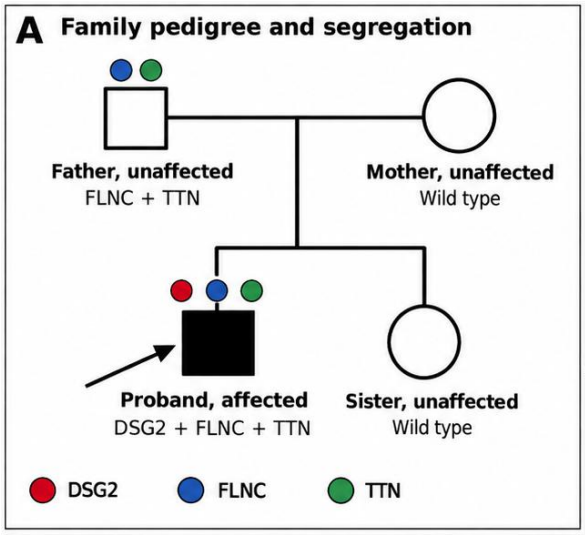

E Genotype and phenotype matrix

Individual	DSG2	FLNC	TTN	Phenotype
Proband	+	+	+	**Affected**
Father	−	+	+	**Unaffected**
Mother	−	−	−	**Unaffected**
Sister	−	−	−	**Unaffected**

Key contrast: the father carries FLNC p.His348Tyr and TTN p.Lys13330Asn without overt cardiomyopathy. The proband additionally carries the DSG2 p.His361Arg variant.

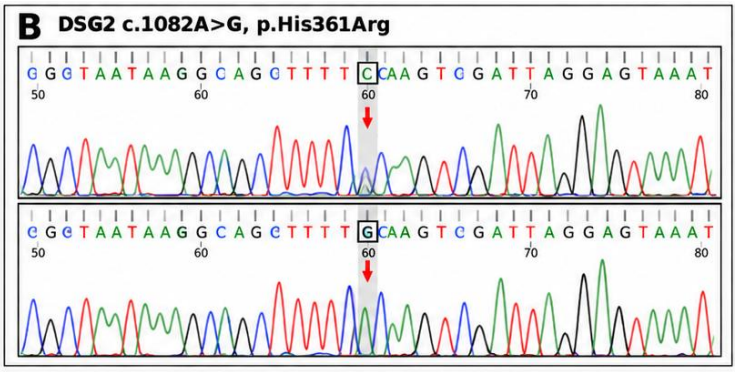

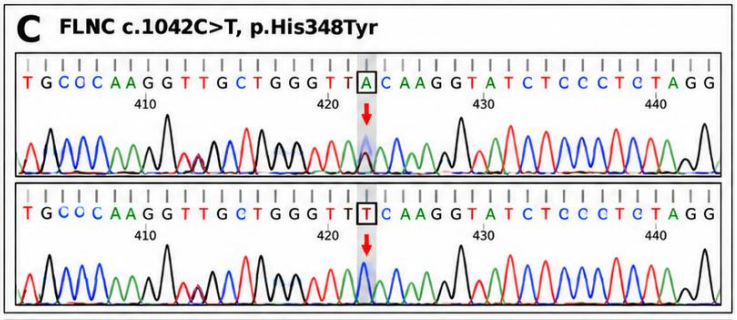

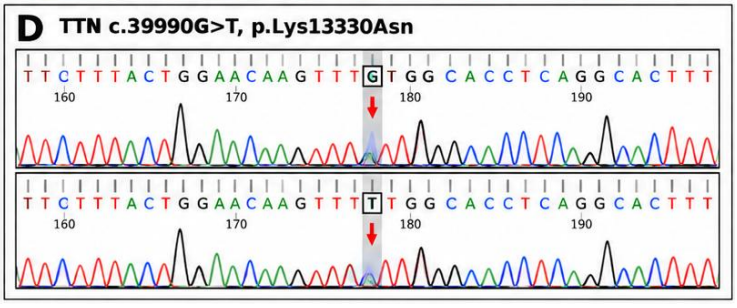

Figure 3. Family segregation and Sanger validation. Panel A is a corrected pedigree reconstructed from the verified family data. Panels B to D are the original Sanger chromatograms for DSG2, FLNC, and TTN, respectively. Panel E summarizes the genotype and phenotype contrast. The chromatograms were not regenerated.

DSG2 conservation and regional structural context

The canonical human DSG2 sequence Q14126 contains the local motif SVIVANKAAFHKSIRSKYKP around His361. Orthologous sequence segments from mouse DSG2 O55111 and pig DSG2 A0A287ATF2 retain the histidine immediately following the conserved NKAAF motif. This limited cross-species comparison supports local sequence conservation of the index residue. The analysis was intentionally restricted to orthologues for which the relevant sequence segment could be directly verified. No broader conservation claim was made.

His361 maps to the extracellular cadherin region of DSG2 and lies within EC3. This location is important because extracellular cadherin domains contribute to calcium-dependent desmosomal adhesion and mechanical stability [7]. A 2026 integrative study found that clinically important DSG2 missense variants are enriched in extracellular domains and described a compound genotype containing the nearby EC3 variant p.Ala358Thr together with p.Ala131Thr. That proband developed symptoms at age 13 and progressed to biventricular disease [8]. The same study also summarized p.Thr335Ala in EC3, although current evidence for that substitution is context dependent and current ClinVar classifications are conflicting. These examples do not establish pathogenicity of p.His361Arg. They show that the immediate EC3 region has prior disease-relevant variation and that variant dosage and genetic background can materially alter phenotype. The position of His361, the local sequence conservation, and the neighboring EC3 variants are illustrated in Fig. 4.

A targeted search of the accessible published literature did not identify a previous report of the exact DSG2 p.His361Arg substitution in arrhythmogenic cardiomyopathy. Therefore, the strongest evidence in the present case comes from the gene-disease validity of DSG2, family segregation, the conserved and structurally relevant local region, the patient phenotype, and the molecular dynamics findings. Exact population frequency should be reconfirmed from the final clinical variant report and the current gnomAD release before formal ACMG criteria are assigned. The evidence supporting the hierarchical interpretation of the three variants is summarized in Table 2.

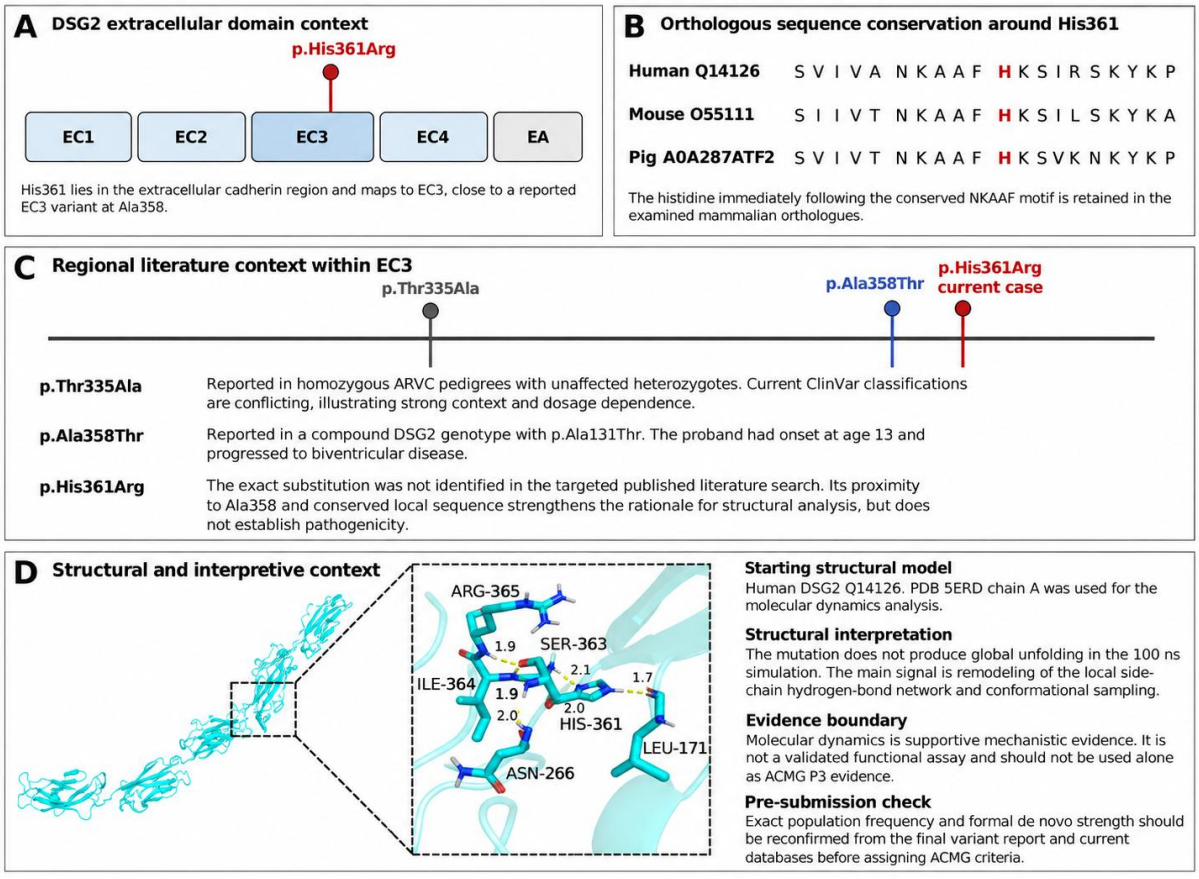

Figure 4. Conservation and regional context of DSG2 p.His361Arg. Panel A places His361 in the extracellular cadherin region. Panel B shows the verified local orthologous sequences from human, mouse, and pig. Panel C places the index variant beside reported EC3 variants p.Thr335Ala and p.Ala358Thr and summarizes their context. Panel

D links the regional evidence to the original DSG2 molecular structure used in the simulation and states the evidentiary boundary of molecular dynamics.

Table 2. Hierarchical interpretation of the three variants. Gene-level evidence, family segregation, and molecular dynamics are separated to avoid conflating biological plausibility with proof of variant pathogenicity.

Gene and variant	Inheritance in this family	External gene-disease context	Structural or MD signal	Working interpretation
DSG2 NM_001943.5:c.1082A>G, p.His361Arg	Present only in proband; compatible with de novo occurrence in tested family	DSG2 has strong/definitive evidence for classical ACM. His361 lies in conserved extracellular EC3. Nearby Ala358 has been reported in severe compound DSG2 disease.	Global fold largely preserved. Local hydrogen-bond network is reduced/reorganized. Early local contacts are altered. Conformational landscape is broader and more connected.	Primary disease-associated candidate. Pathogenicity of this exact substitution remains to be functionally validated.
FLNC NM_001458.5:c.1042C>T, p.His348Tyr	Paternally inherited; father clinically unaffected	FLNC truncating variants are established causes of high-risk dilated and arrhythmogenic cardiomyopathy. Evidence cannot be directly extrapolated to an unvalidated missense variant.	Local RMSF is lower. Local hydrogen bonding and close contacts increase. Global fold remains stable.	Candidate modifier. Independent causality is not established.
TTN NM_001267550.2:c.39990G>T, p.Lys13330Asn	Paternally inherited; father clinically unaffected	TTN is established in dilated cardiomyopathy. ClinGen currently classifies the TTN to classical ARVC gene-disease relationship as disputed.	Within the 86-residue modeled fragment, local hydrogen bonding increases and the free-energy landscape broadens. Global structural measures remain similar.	Candidate modifier only. The result should not be interpreted as evidence that TTN independently caused ARVC.

Molecular Dynamics Results

DSG2 p.His361Arg: global stability is preserved while local interactions are remodeled

The DSG2 wild-type and mutant systems both reached a dynamic regime during the 100 ns simulation. The mutant showed a modestly higher backbone root mean square deviation and

somewhat greater fluctuations, but the trajectory did not indicate catastrophic unfolding. Whole-protein root mean square fluctuation profiles were broadly similar. Radius of gyration, solvent-accessible surface area, and global intramolecular hydrogen-bond counts also converged to broadly comparable ranges. These global descriptors argue against a model in which p.His361Arg simply destabilizes the entire ectodomain.

The most informative differences were local. In the wild-type system, HIS361 formed approximately five to six hydrogen bonds with surrounding residues during the later phase of the trajectory. ARG361 in the mutant generally formed fewer local hydrogen bonds, approximately three to four after local equilibration. Contacts within 0.35 nm were initially lower in the mutant. A transient reorganization occurred during approximately 25 to 45 ns, followed by later convergence toward the wild-type contact scale. The interpretation is therefore not loss of all local packing. Instead, p.His361Arg changes the interaction network and the pathway by which the local microenvironment reaches equilibrium.

Representative structures provide a direct side-chain explanation. In the wild type, HIS361 formed hydrogen bonds with LEU171, ASN266, SER363, ILE364, and ARG365, with observed distances of approximately 1.7 to 2.1 Å. In the mutant, ARG361 interacted with ASN266, ILE364, and ARG365, with distances of approximately 2.1 to 2.6 Å. Histidine and arginine differ substantially in side-chain geometry, charge state, and hydrogen-bonding capacity. The substitution therefore remodels the local network even though the backbone remains largely preserved. The global and local dynamic changes associated with DSG2 p.His361Arg are illustrated in Fig. 5.

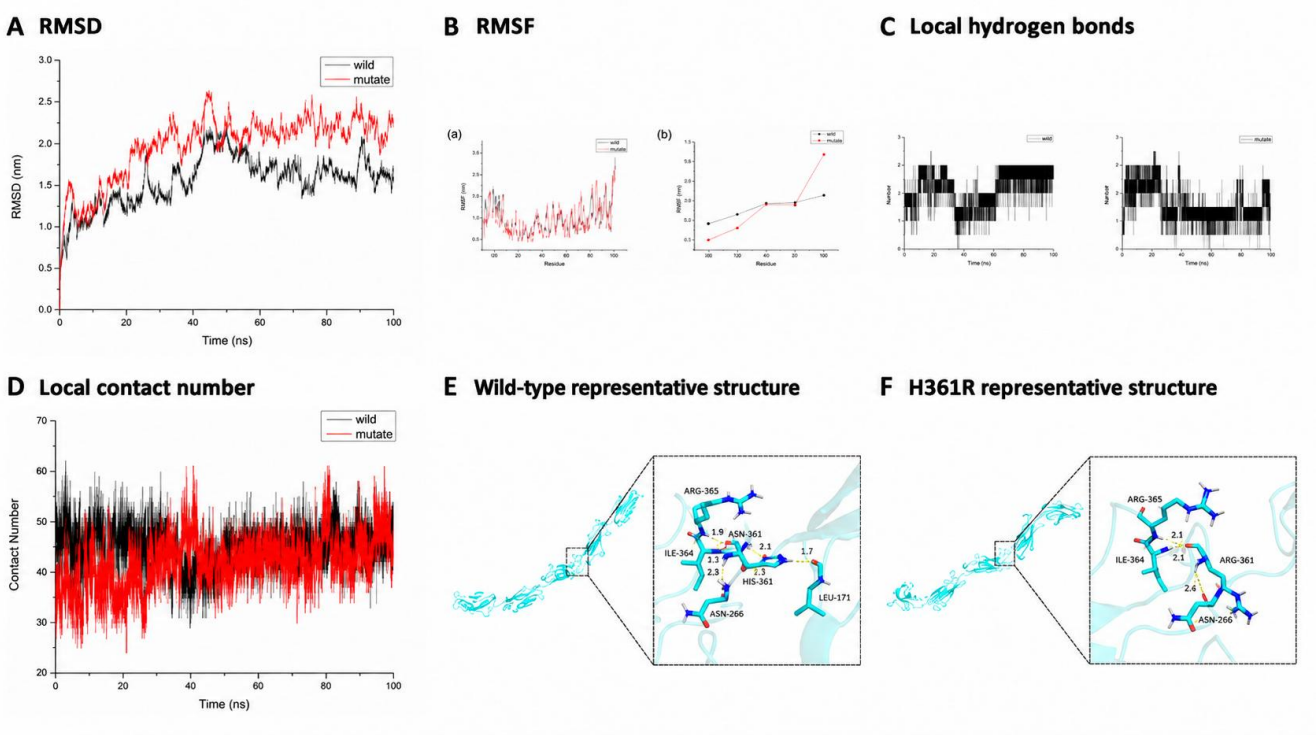

306

307 **Figure 5.** Local and global molecular dynamics of DSG2 p.His361Arg using the original simulation outputs. The
308 figure includes backbone RMSD, RMSF, local hydrogen bonds, local contact number, and representative wild-type
309 and mutant structures. No occupancy values or other uncalculated summary statistics were added.

310 **DSG2 p.His361Arg: conformational sampling is altered without major secondary-structure**
311 **collapse**

312 Principal-component and free-energy analysis provided a second layer of evidence. The wild-
313 type protein sampled relatively separated low-energy conformational states. The mutant occupied
314 a broader and more connected conformational space, with shallow interconnecting regions
315 between low-energy states. This pattern is consistent with increased conformational
316 heterogeneity and easier transitions among accessible substates. It is a change in the
317 conformational ensemble rather than evidence of wholesale unfolding.

318 Secondary-structure analysis further supports this distinction. Coil content changed only from
319 0.27 in the wild type to 0.29 in the mutant. Beta-sheet content changed from 0.42 to 0.41. Other

secondary-structure components differed minimally. His361 is located in a beta-sheet-associated extracellular cadherin region, but the mutation did not trigger a major beta-sheet to coil transition. The mechanistic signal is therefore concentrated in side-chain interactions and collective dynamics. This directly addresses the apparent discrepancy between limited global structural change and potentially meaningful molecular consequences. The free-energy landscapes, secondary-structure evolution, and representative conformations are presented in Fig. 6.

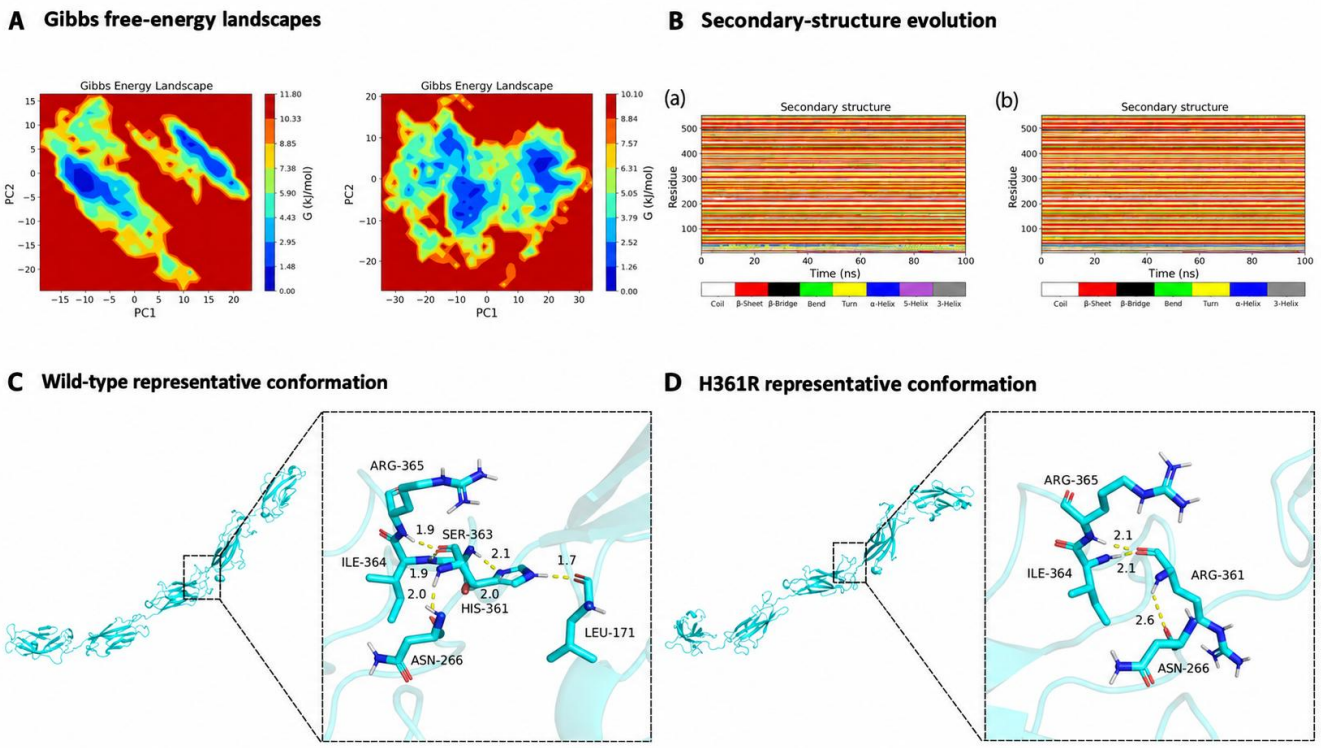

Figure 6. Conformational landscape and secondary-structure analysis of DSG2. The original Gibbs free-energy landscapes, secondary-structure evolution plots, and representative low-energy structures are shown. Wild-type and mutant outputs are interpreted as evidence of altered conformational sampling with preservation of the overall secondary-structure framework.

FLNC p.His348Tyr and TTN p.Lys13330Asn: distinct local dynamic signatures

The FLNC simulation showed a different pattern. Global RMSD, solvent exposure, overall hydrogen bonding, and secondary-structure composition remained broadly stable. Around

residue 348, however, local root mean square fluctuation was lower in the mutant. TYR348 formed more local hydrogen bonds and showed greater close-contact density than HIS348. Representative mutant structures showed interactions with VAL366, VAL344, LYS343, and GLY346, whereas the wild-type HIS348 showed two hydrogen bonds with VAL366. The free-energy landscape also shifted toward a more connected dominant basin. Together, these findings are more consistent with local rigidification and altered local adaptability than with global destabilization.

The TTN analysis must be interpreted more narrowly because only an 86-residue fragment spanning residues 13,299 to 13,384 was modeled. The full-length Lys13330 corresponds to residue 32 of the simulated fragment. Global RMSD, radius of gyration, solvent exposure, global hydrogen bonding, contact number, and beta-sheet content were broadly similar between systems. At the variant site, ASN13330 formed hydrogen bonds more frequently than LYS13330 and transiently reached approximately five local hydrogen bonds around 40 ns. The mutant free-energy landscape was broader and more anisotropic, with an elongated low-energy region and a branch-like extension. These data support altered local polar interactions and conformational sampling within the modeled fragment. They cannot be generalized to the mechanics of full-length titin. The distinct dynamic patterns of the inherited FLNC and TTN variants are shown in Fig. 7. A comparison of the molecular dynamics findings across all three proteins is provided in Table 3.

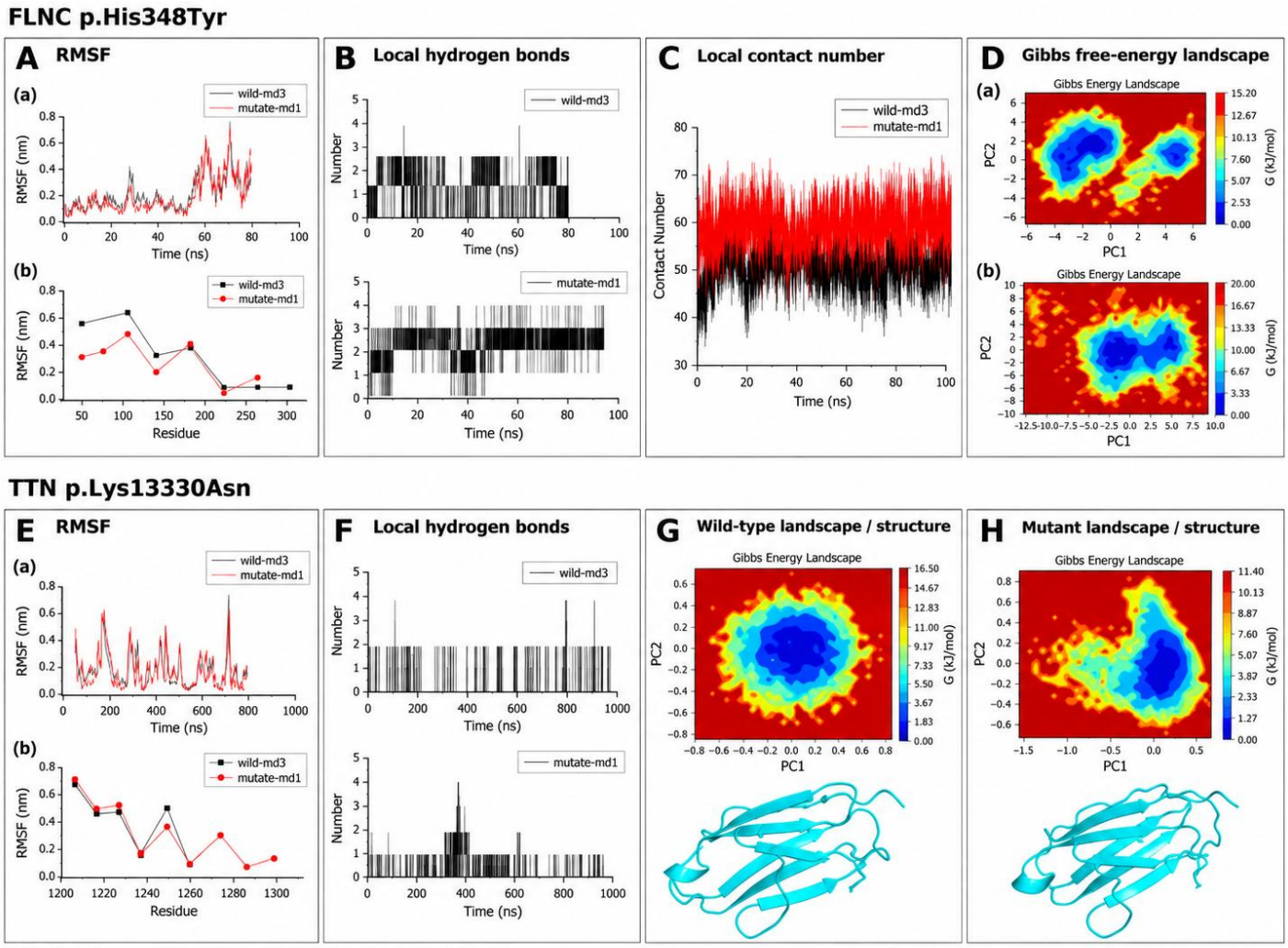

353

354 **Figure 7.** Molecular dynamics of the inherited FLNC and TTN variants using the original simulation outputs. Panels
355 A to D summarize the FLNC p.His348Tyr local dynamic signature. Panels E to H summarize TTN p.Lys13330Asn
356 within the modeled fragment. The results are presented as potential modifier-related molecular effects and not as
357 proof of independent pathogenicity.

Table 3. Integrated molecular dynamics interpretation. The table distinguishes global stability metrics from the local and conformational signals that carry the main mechanistic information.

Protein	Global behavior	Local behavior at variant site	Conformational landscape	Mechanistic interpretation
DSG2 p.His361Arg	No gross unfolding. Rg, SASA, global H bonds, and secondary structure broadly preserved.	Fewer/reorganized H bonds around residue 361; early local contact density reduced before re-equilibration.	Broader and more connected low-energy sampling.	Local interaction destabilization and altered state sampling despite preservation of the global fold.
FLNC p.His348Tyr	Overall stability and secondary structure broadly preserved.	Lower local RMSF; increased H bonding and close contacts.	More connected dominant basin.	Local rigidification and altered cytoskeletal dynamic adaptability.
TTN p.Lys13330Asn	Modeled 86-residue fragment remains globally stable; local contact scale and beta-sheet content preserved.	Increased local hydrogen-bonding frequency with similar close-contact number.	Broader and more anisotropic landscape.	Altered local polar interactions and collective sampling within the fragment.

Integrated Genotype-Phenotype Interpretation

The clinical and genetic data form a coherent hierarchy. First, the phenotype is unusually severe for age. Exercise-associated syncope preceded the diagnosis by five years. By age 22, the patient had a high ventricular ectopic burden, ventricular tachycardia, profound right ventricular systolic failure, and measurable left ventricular dysfunction. Second, the family provides an internal genetic contrast. The father carries the same FLNC and TTN variants but has no overt cardiomyopathy, whereas the proband carries those two variants plus DSG2 p.His361Arg and has severe disease. Third, the molecular dynamics data show the clearest disease-relevant perturbation for DSG2 at the level of the local interaction network and conformational landscape. These observations support an oligogenic modifier hypothesis, but they do not prove epistasis. The most defensible interpretation is that DSG2 p.His361Arg is the principal disease-associated candidate because it occurs in a definitively associated ACM gene, is present only in the proband within the tested family, lies in a conserved extracellular cadherin region, is close to a reported

severe-disease EC3 variant, and produces a coherent local dynamic disturbance. FLNC p.His348Tyr and TTN p.Lys13330Asn may influence mechanical background or cellular reserve, but the father demonstrates that they are not sufficient to produce the observed phenotype in this family under the available clinical evaluation.

The modifier hypothesis is also consistent with published genotype-complexity studies. Compound and digenic desmosomal genotypes have been repeatedly associated with earlier disease expression, greater penetrance, or more severe arrhythmic outcomes [11]. Additional variants increased disease penetrance among mutation-positive relatives in a large family study [12]. Multiple-mutation carriers had greater left ventricular involvement in an Italian series [13]. Complex desmosomal genotypes were also associated with adverse lifetime arrhythmic outcomes [14]. Importantly, these studies largely concern established desmosomal variants and cannot be used to assign pathogenicity to the present FLNC or TTN missense variants. They instead provide a conceptual precedent for genetic-background effects. The proposed relationships among DSG2, the candidate modifier variants, and the biventricular phenotype are illustrated in Fig. 8.

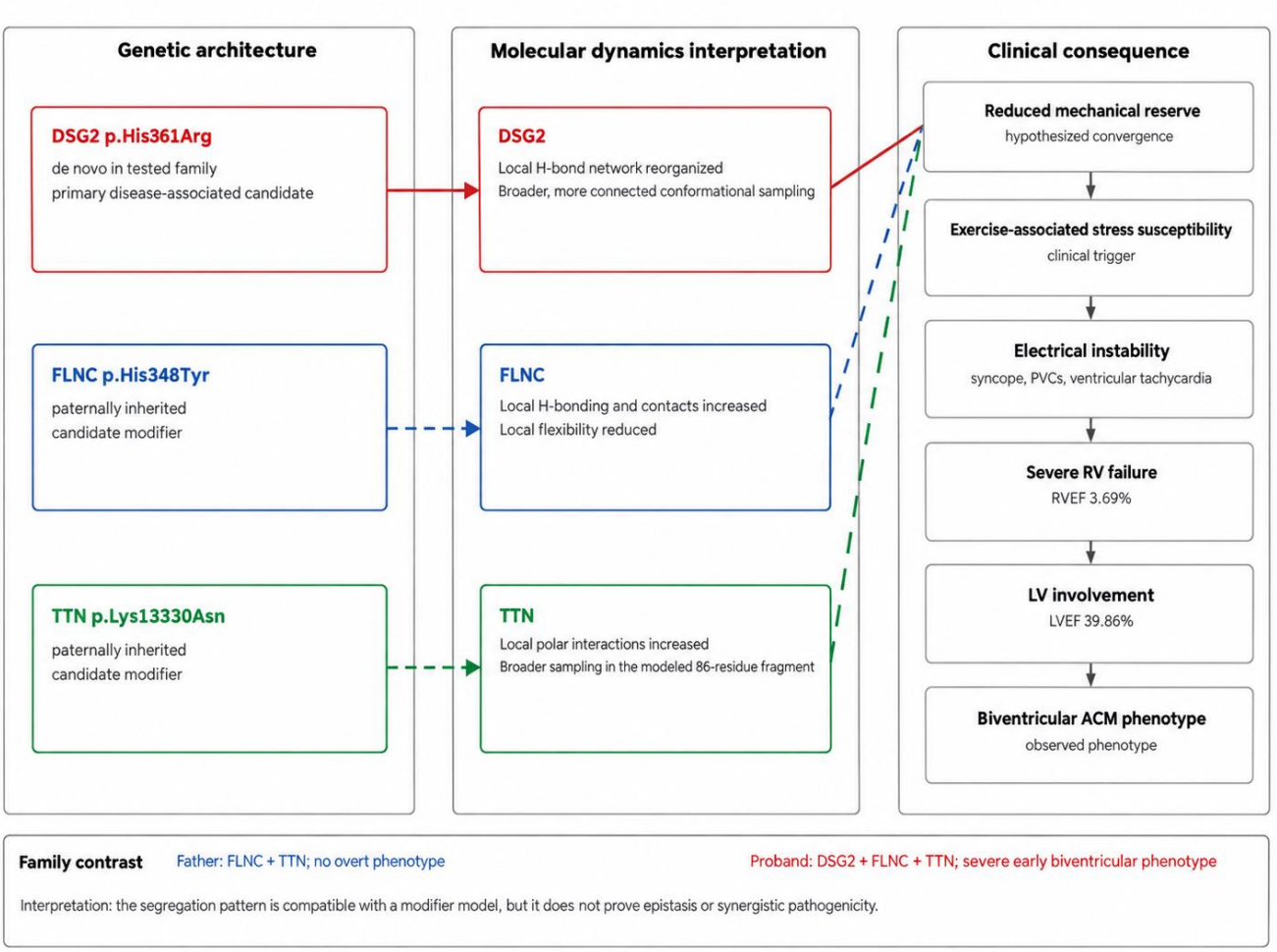

Figure 8. Proposed oligogenic modifier model. The solid red pathway represents the principal DSG2 hypothesis. Dashed pathways represent the candidate modifier roles of FLNC and TTN. The family contrast is shown explicitly. This figure is a mechanistic hypothesis derived from the integrated clinical, segregation, literature, and molecular dynamics evidence and is not presented as direct experimental proof of epistasis.

Discussion

This report was substantially restructured to answer a specific mechanistic question: how can a newly identified DSG2 missense variant and two paternally inherited variants be interpreted in a young patient with exceptionally severe biventricular arrhythmogenic cardiomyopathy? The earlier manuscript treated the three genes too similarly. That approach was not supported by

current gene-disease evidence. The revised analysis separates a primary DSG2 signal from two possible background modifiers and requires each level of the proposed model to be supported by a different type of evidence.

The DSG2 evidence is the strongest. DSG2 is a validated arrhythmogenic cardiomyopathy gene [5]. The protein is a cardiac desmosomal cadherin whose extracellular domains mediate mechanically important intercellular adhesion [7]. His361 is conserved in the examined mammalian orthologues and lies in EC3. This is close to p.Ala358Thr, which was recently described in a compound DSG2 genotype associated with onset at age 13 and progression to biventricular disease [8]. The relevance of this comparison is regional rather than variant specific. It indicates that the local EC3 architecture is clinically meaningful. It does not imply that all substitutions in the region are pathogenic. The p.Thr335Ala example is particularly instructive because severe disease has been reported in homozygotes while heterozygotes may remain unaffected, and its current clinical classification remains contested. This reinforces the broader principle that sequence location, dosage, and genetic background must be interpreted together.

The molecular dynamics results resolve another important issue. A missense variant does not need to unfold an entire protein to have a functional consequence. DSG2 p.His361Arg produced only small changes in global stability and secondary-structure composition. The decisive changes were local. The hydrogen-bond network around residue 361 was reduced and reorganized. Early local packing changed. The mutant sampled a broader and more connected free-energy landscape. This pattern is mechanistically plausible for a surface or domain-level missense substitution. Experimental studies of desmosomal cadherins have shown that disease-associated substitutions can alter binding kinetics even when a canonical binding motif or gross structure is preserved [9]. Similar observations have been reported for other desmosomal proteins. Molecular dynamics

analysis of arrhythmogenic cardiomyopathy-associated desmoplakin variants showed that local interface mechanics and flexibility can be altered without a uniform global structural phenotype [29]. In a complementary desmoplakin study, molecular dynamics revealed no overt global structural change but identified loss of local intramolecular interactions that was subsequently linked experimentally to increased proteolytic susceptibility [30]. These studies provide an appropriate benchmark for interpreting the present DSG2 result. The relevant signal is local dynamic remodeling, not dramatic global denaturation.

The FLNC and TTN findings require more restraint. FLNC truncating variants are well established in high-risk dilated and arrhythmogenic cardiomyopathy [15]. Truncating FLNC variants have also been reported in right ventricular arrhythmogenic cardiomyopathy [16]. The present p.His348Tyr substitution is a missense variant, so the evidence from truncating variants cannot be transferred directly. Its simulation signature suggests local rigidification because hydrogen bonding and close contacts increased while local fluctuation decreased. This could plausibly influence the dynamic behavior of an actin-crosslinking protein, but no direct cellular consequence was measured. TTN requires even greater caution. Although titin is central to sarcomeric mechanics and TTN truncating variants are a major cause of dilated cardiomyopathy [17], the current ClinGen classification for TTN and classical arrhythmogenic right ventricular cardiomyopathy is disputed [18]. In addition, only a short local TTN fragment was simulated. The observed increase in local hydrogen bonding and broader conformational sampling can therefore support only a candidate modifier interpretation.

The family segregation pattern is what gives these modest molecular effects clinical relevance. The father shares FLNC p.His348Tyr and TTN p.Lys13330Asn but has no overt cardiomyopathy, while the proband also carries DSG2 p.His361Arg and developed severe disease at a young age.

This is compatible with a threshold model in which a primary desmosomal perturbation acts on a background with altered cytoskeletal or sarcomeric dynamics. It is also compatible with incomplete penetrance, age-dependent expression, unmeasured environmental effects, or additional genetic variation not captured by the proposed model. Accordingly, the terms modifier and oligogenic should remain hypotheses rather than conclusions of causality.

The clinical implications remain important even if the molecular model is not yet proven. The patient had exercise-associated syncope, documented ventricular tachycardia, a very high ectopic burden, and profound right ventricular dysfunction. Contemporary arrhythmogenic cardiomyopathy guidance emphasizes avoidance of high-intensity exercise and careful sudden-death risk assessment [3]. An implantable cardioverter-defibrillator was recommended in the source clinical record but was declined. Continued pharmacological therapy, exercise restriction, rhythm surveillance, ventricular-function monitoring, and family follow-up are therefore particularly important. The father should not be considered definitively unaffected for life solely because overt disease was not present at the time of assessment. Age-dependent penetrance and subtle phenotypes remain possible.

Finally, computational evidence must be kept within its evidentiary limits. The molecular dynamics results strengthen biological plausibility and help prioritize mechanisms for future experiments. They do not constitute a validated functional assay by themselves. ClinGen guidance for the ACMG PS3 and BS3 criteria requires well-established functional assays with appropriate controls and validation [31]. Formal sequence-variant classification should therefore follow the ACMG and AMP framework and should incorporate verified population frequency, segregation, de novo status, phenotype specificity, and validated functional evidence where

available [32]. In the present case, the safest conclusion is that the computational findings support, but do not prove, the proposed DSG2-centered oligogenic model.

Limitations

Several limitations should be stated explicitly. First, no cardiomyocyte, tissue, or animal experiment was performed to test desmosomal adhesion, protein localization, degradation, or mechanotransduction. Second, the apparent de novo DSG2 event is based on family testing; confirmation of biological parentage was not documented in the supplied materials. Third, the father was described as clinically unaffected, but the depth and duration of his cardiac phenotyping were not fully documented. Fourth, one 100 ns production trajectory per wild-type or mutant system was available, without independent replicate trajectories. The molecular dynamics differences therefore should not be treated as replicate-level statistical effects. Fifth, the TTN analysis involved an 86-residue modeled fragment rather than full-length titin. Sixth, exact current population frequencies for the three variants should be reconfirmed from the final clinical variant report and current population databases before manuscript submission. These limitations do not invalidate the mechanistic observations, but they substantially limit claims of causality and synergy.

Conclusion

A severe early biventricular arrhythmogenic cardiomyopathy phenotype was observed in a young man carrying DSG2 p.His361Arg together with paternally inherited FLNC p.His348Tyr and TTN p.Lys13330Asn. The revised evidence hierarchy supports DSG2 as the principal disease-associated candidate. His361 is conserved in the examined mammalian orthologues, lies in a disease-relevant extracellular cadherin region, and is close to a reported EC3 variant associated

with severe compound DSG2 disease. Molecular dynamics further shows that p.His361Arg preserves the global fold but remodels local hydrogen bonding and conformational sampling. FLNC and TTN show distinct local dynamic effects but remain candidate modifiers because they are inherited from an unaffected father and because their variant-level disease evidence is limited. Functional studies are required to validate the proposed oligogenic mechanism.

Declarations

Ethics approval and consent to participate: The study was conducted in accordance with the Declaration of Helsinki and was approved by the Medical Ethics Review Committee of the Second Hospital of Jilin University (Approval No. 2026-419; approval date: 22 October 2026). Written informed consent to participate in the study was obtained from all four participants, including the proband, his father, his mother, and his sister.

Consent for publication: Written informed consent for publication of the relevant clinical, genetic, electrocardiographic, and imaging data was obtained from all four participants (the proband, his father, mother, and sister).

Availability of data and materials: The datasets generated and/or analysed during the current study are available in the Genome Sequence Archive-Human (GSA-Human) repository with accession number HRA022219: https://ngdc.cncb.ac.cn/gsa-human/s/1M0mNE5E.

Competing interests: The authors declare that they have no competing interests.

Funding: This work was supported by the Science and Technology Development Program of Jilin Province (Science and Technology Resources Development Project, Grant No. 20250206005ZP).

Author contributions: Ming Zhang: Conceptualization, clinical data collection, data analysis, visualization, writing – original draft. Ziyuan Guo: Conceptualization, genetic data analysis,

molecular dynamics simulation, visualization, writing – original draft. Lirui Kang: Clinical investigation, patient management, and clinical data collection. Tianyi Li: Genetic variant interpretation and bioinformatics analysis. Yinuo Guan: Molecular dynamics analysis and visualization. Kang LV: Data curation, literature review, and manuscript revision. Ziyan Jiao: Clinical supervision, data interpretation, and writing – review & editing. Jichang Zhang: Conceptualization, methodology, supervision, project administration, and writing – review & editing.

References

1. Corrado D, Perazzolo Marra M, Zorzi A, et al. Diagnosis of arrhythmogenic cardiomyopathy: The Padua criteria. Int J Cardiol. 2020;319:106-114. doi:10.1016/j.ijcard.2020.06.005.
2. Marcus FI, McKenna WJ, Sherrill D, et al. Diagnosis of arrhythmogenic right ventricular cardiomyopathy/dysplasia: proposed modification of the Task Force Criteria. Eur Heart J. 2010;31(7):806-814. doi:10.1093/eurheartj/ehq025.
3. Towbin JA, McKenna WJ, Abrams DJ, et al. 2019 HRS expert consensus statement on evaluation, risk stratification, and management of arrhythmogenic cardiomyopathy. Heart Rhythm. 2019;16(11):e301-e372. doi:10.1016/j.hrthm.2019.05.007.
4. Arbelo E, Protonotarios A, Gimeno JR, et al. 2023 ESC Guidelines for the management of cardiomyopathies. Eur Heart J. 2023;44(37):3503-3626. doi:10.1093/eurheartj/ehad194.
5. James CA, Jongbloed JDH, Hershberger RE, et al. International evidence based reappraisal of genes associated with arrhythmogenic right ventricular cardiomyopathy using the Clinical Genome Resource framework. Circ Genom Precis Med. 2021;14(3):e003273. doi:10.1161/CIRCGEN.120.003273.

6. Awad MM, Dalal D, Cho E, et al. DSG2 mutations contribute to arrhythmogenic right ventricular dysplasia/cardiomyopathy. Am J Hum Genet. 2006;79(1):136-142. doi:10.1086/504393.

7. Harrison OJ, Brasch J, Lasso G, et al. Structural basis of adhesive binding by desmocollins and desmogleins. Proc Natl Acad Sci U S A. 2016;113(26):7160-7165. doi:10.1073/pnas.1606272113.

8. Pinci S, Celeghin R, Martini M, et al. Integrative genomic and literature assessment of desmoglein 2-related arrhythmogenic cardiomyopathy with Italian cohort validation. Commun Med. 2026;6(1):145. doi:10.1038/s43856-026-01416-w.

9. Dieding M, Debus JD, Kerkhoff R, et al. Arrhythmogenic cardiomyopathy related DSG2 mutations affect desmosomal cadherin binding kinetics. Sci Rep. 2017;7:13791. doi:10.1038/s41598-017-13737-x.

10. Göz M, et al. Arrhythmogenic cardiomyopathy-related cadherin variants affect desmosomal binding kinetics. J Mol Cell Cardiol. 2024;195:36-44. doi:10.1016/j.yjmcc.2024.07.009.

11. Xu T, Yang Z, Vatta M, et al. Compound and digenic heterozygosity contributes to arrhythmogenic right ventricular cardiomyopathy. J Am Coll Cardiol. 2010;55(6):587-597. doi:10.1016/j.jacc.2009.11.020.

12. Quarta G, Muir A, Pantazis A, et al. Familial evaluation in arrhythmogenic right ventricular cardiomyopathy: impact of genetics and revised task force criteria. Circulation. 2011;123(23):2701-2709. doi:10.1161/CIRCULATIONAHA.110.976936.

13. Bauce B, Nava A, Beffagna G, et al. Multiple mutations in desmosomal proteins encoding genes in arrhythmogenic right ventricular cardiomyopathy/dysplasia. Heart Rhythm. 2010;7(1):22-29. doi:10.1016/j.hrthm.2009.09.070.

14. Rigato I, Bauce B, Rampazzo A, et al. Compound and digenic heterozygosity predicts lifetime arrhythmic outcome and sudden cardiac death in desmosomal gene-related arrhythmogenic right ventricular cardiomyopathy. Circ Cardiovasc Genet. 2013;6(6):533-542. doi:10.1161/CIRCGENETICS.113.000288.

15. Ortiz-Genga MF, Cuenca S, Dal Ferro M, et al. Truncating FLNC mutations are associated with high-risk dilated and arrhythmogenic cardiomyopathies. J Am Coll Cardiol. 2016;68(22):2440-2451. doi:10.1016/j.jacc.2016.09.927.

16. Brun F, Gigli M, Graw SL, et al. FLNC truncations cause arrhythmogenic right ventricular cardiomyopathy. J Med Genet. 2020;57(4):254-257. doi:10.1136/jmedgenet-2019-106394.

17. Herman DS, Lam L, Taylor MRG, et al. Truncations of titin causing dilated cardiomyopathy. N Engl J Med. 2012;366(7):619-628. doi:10.1056/NEJMoa1110186.

18. ClinGen Hereditary Cardiovascular Disease Gene Curation Expert Panel. TTN-arrhythmogenic right ventricular cardiomyopathy gene-disease validity: Disputed. Clinical Genome Resource. Classification dated October 28, 2025. Accessed October 6, 2026.

19. te Riele ASJM, Tandri H, Bluemke DA. Arrhythmogenic right ventricular cardiomyopathy: cardiovascular magnetic resonance update. J Cardiovasc Magn Reson. 2014;16:50. doi:10.1186/s12968-014-0050-8.

20. Camm CF, James CA, Tichnell C, et al. Premature ventricular contraction variability in arrhythmogenic right ventricular dysplasia/cardiomyopathy. J Cardiovasc Electrophysiol. 2015;26(1):53-57. doi:10.1111/jce.12544.

21. Platonov PG, Calkins H, Hauer RNW, et al. High interobserver variability in the assessment of epsilon waves: implications for diagnosis of arrhythmogenic right ventricular

578 cardiomyopathy/dysplasia. Heart Rhythm. 2016;13(1):208-216.
579 doi:10.1016/j.hrthm.2015.08.031.
580 22. Waterhouse A, Bertoni M, Bienert S, et al. SWISS-MODEL: homology modelling of protein
581 structures and complexes. Nucleic Acids Res. 2018;46(W1):W296-W303.
582 doi:10.1093/nar/gky427.
583 23. Pettersen EF, Goddard TD, Huang CC, et al. UCSF Chimera: a visualization system for
584 exploratory research and analysis. J Comput Chem. 2004;25(13):1605-1612.
585 doi:10.1002/jcc.20084.
586 24. Schrödinger LLC. The PyMOL Molecular Graphics System. Version 2.0. Schrödinger LLC;
587 2020.
588 25. Abraham MJ, Murtola T, Schulz R, et al. GROMACS: high performance molecular
589 simulations through multi-level parallelism from laptops to supercomputers. SoftwareX.
590 2015;1-2:19-25. doi:10.1016/j.softx.2015.06.001.
591 26. Bussi G, Donadio D, Parrinello M. Canonical sampling through velocity rescaling. J Chem
592 Phys. 2007;126(1):014101. doi:10.1063/1.2408420.
593 27. Parrinello M, Rahman A. Polymorphic transitions in single crystals: a new molecular
594 dynamics method. J Appl Phys. 1981;52(12):7182-7190. doi:10.1063/1.328693.
595 28. Essmann U, Perera L, Berkowitz ML, Darden T, Lee H, Pedersen LG. A smooth particle
596 mesh Ewald method. J Chem Phys. 1995;103(19):8577-8593. doi:10.1063/1.470117.
597 29. Daday C, Mateyka LM, Gräter F. How ARVC-related mutations destabilize desmoplakin: an
598 MD study. Biophys J. 2019;116(5):831-835. doi:10.1016/j.bpj.2019.01.023.

30. Ng R, Manring H, Papoutsidakis N, et al. Patient mutations linked to arrhythmogenic cardiomyopathy enhance calpain-mediated desmoplakin degradation. JCI Insight. 2019;5(14):e128643. doi:10.1172/jci.insight.128643.

31. Brnich SE, Abou Tayoun AN, Couch FJ, et al. Recommendations for application of the functional evidence PS3/BS3 criterion using the ACMG/AMP sequence variant interpretation framework. Genome Med. 2020;12(1):3. doi:10.1186/s13073-019-0690-2.

32. Richards S, Aziz N, Bale S, et al. Standards and guidelines for the interpretation of sequence variants: a joint consensus recommendation of the ACMG and AMP. Genet Med. 2015;17(5):405-424. doi:10.1038/gim.2015.30.